BUOYANCY INDUCED 3D-TRANSITION BEHIND A HEATED CYLINDER

M. Ren, C.C.M Rindt and A.A. van Steenhoven
Laboratory for Energy Technology, Department of Mechanical Engineering
Eindhoven University of Technology
P.O.Box 513, 5600 MB Eindhoven, The Netherlands
m.ren@tue.nl, c.c.m.rindt@tue.nl and a.a.v.steenhoven@tue.nl

ABSTRACT

3D-transition behind a heated cylinder is studied at low Reynolds numbers. Both experimental and numerical techniques are used, including an electro-chemical tin-precipitation visualization method and a 3D Spectral Element Method. It is observed that 3D vortical structures are formed directly behind the cylinder. Distinct counter-rotating vortices are observed and they are associated with a non-uniform temperature distribution along the spanwise direction in the near-wake. These vortices induce thermal plumes to escape from the upper braid in the far-wake.

INTRODUCTION

It is well-known that the earliest recorded observation of the vortex shedding phenomenon can be traced back to the sixteenth century when Leonardo da Vinci made drawings of the surface pattern of the flow past an obstacle. Bluff body wake flows have direct engineering significance. The formation of vortices behind bluff bodies is important since they determine not only the drag but also the heat transfer to the environment.

From a fundamental point of view, the study of the instability mechanisms resulting in the formation of 2D and 3D vortical structures, can contribute to the understanding of laminar-turbulent transition and lead to ways to actively control the features of the flow. When the cylinder is not heated, 3D-transition of the wake flow takes place at a Reynolds number of around 190. The von Kármán vortex street becomes unstable and irregular, and the flow within the vortices themselves becomes chaotic. Two modes of small-scale 3D instability have been described as mode-A and mode-B instability (Williamson 1996).

For low Reynolds number flow around a heated cylinder, the strength of the buoyancy induced convection flow can be of the same order of magnitude as the forced convection flow (Kieft *et al.* 2002; 2003). The interaction between these two types of convection changes the mixing properties of the flow compared to the purely forced convection case. This mixing process is of interest in several applications, for example, in electronics cooling, where the flow behind a cooled component strongly influences the cooling behavior of downstream placed components.

Recent visualization results show that, when the cylinder is heated, a 3D-transition in the wake flow occurs at a lower Reynolds number than in the unheated case (Maas *et al.* 2003). From visualizations at $Re = 117$ it appeared that for $Ri > 1$ thermal plumes occur in the far-wake, as shown in Figure 3 (c). It is observed that the thermal plumes escape from the upper braid. The spanwise distance between the plumes, observed by a top-view visualization, is around twice the cylinder diameter (Ren *et al.* 2002).

In the present paper, the 3D-transition behind a heated cylinder is studied at low Reynolds numbers. Distinct counter-rotating vortices are observed and they are associated with a non-uniform temperature distribution along the spanwise direction in the near-wake. Both experimental and numerical techniques are used, including an electro-chemical tin-precipitation visualization method and a 3D Spectral Element Method (3D-SEM). The paper is organized as follows. In the next section a description of the problem definition is given, together with the experimental set-up and investigation techniques. After that, observations of 3D-transition behind heated cylinder are presented. Furthermore, 3D-SEM simulation results are presented and a buoyancy induced 3D-transition mechanism in the near-wake is analyzed. Finally, the main conclusions are given.

EXPERIMENTAL SET-UP & TECHNIQUES

Problem definition

In the current investigation a buoyancy induced 3D transition behind a heated cylinder is investigated at low Reynolds numbers. The cylinder is exposed to a horizontal uniform crossflow (Figure 1, where the z-axis is the spanwise direction, the x-axis is the streamwise direction and the cylinder is positioned at $x = 0$).

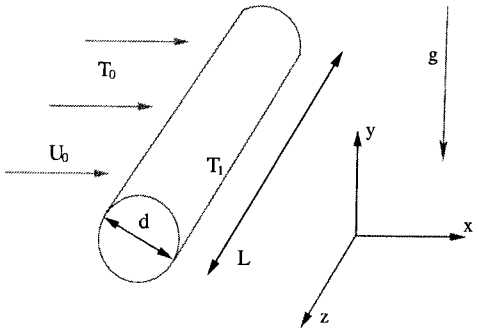

Figure 1: Problem definition.

In the calculations, the flow is assumed to obey the Boussinesq approximation; the density variations are negligible except in the buoyancy force. The dimensionless conservation equations for mass, momentum and energy are respectively:

$$\nabla \cdot \mathbf{u} = 0, \tag{1}$$

$$\frac{\partial \mathbf{u}}{\partial t} + \mathbf{u} \cdot \nabla \mathbf{u} = -\nabla p + \frac{1}{Re} \nabla^2 \mathbf{u} - Ri\, \Theta\, \mathbf{g}, \tag{2}$$

$$\frac{\partial \Theta}{\partial t} + \mathbf{u} \cdot \nabla \Theta = \frac{1}{RePr} \nabla^2 \Theta, \tag{3}$$

with $Re = U_0 d/\nu$ the Reynolds number, $Ri = Gr/Re^2 = g\beta\Delta T d/{U_0}^2$ the Richardson number, $Gr = g\beta\Delta T d^3/\nu^2$

the Grashof number, $Pr = \nu/\kappa$ the Prandtl number, β the expansion coefficient, κ the thermal diffusivity, g the gravity constant, $\mathbf{g}= (0,-1,0)^T$ the dimensionless gravity vector, $\Theta = (T - T_1)/(T_0 - T_1)$ the dimensionless temperature, $\mathbf{u}$ the dimensionless velocity and p the dimensionless pressure. From these dimensionless conservation equations with suitable boundary conditions, one can conclude that the character of the flow depends on the dimensionless parameters Re, Ri and Pr. In the current investigation, Ri is varied between 0 and 1.5, while Re is varied from 70 to 130. The Prandtl number is around 7 because water is used as the working fluid.

Experimental set-up

The apparatus used in the experiment consists of three parts: the water tank, the light source and illumination system, and the image recording and post-processing system.

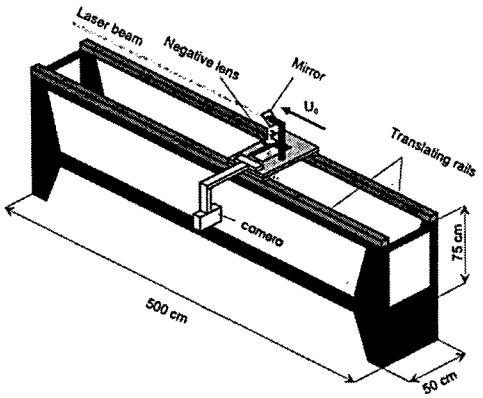

Figure 2: Experimental set-up.

The flow is investigated in a so-called towing tank configuration, as shown in Figure 2, with dimensions $length \times width \times height = 500 \times 50 \times 75$ [cm^3]. In this configuration the cylinder is towed through the water with a constant velocity U_0. The cylinder has length $l = 495$ $[mm]$ and diameter $d = 8.5$ $[mm]$ (aspect ratio $l/d = 58$). A detailed description of the water tank is given by Kieft *et al.* (2002).

For the light source, a pulsed Nd:YAG laser is used. The laser emits light with a wavelength of 532 $[nm]$. One laser pulse has a duration of $6[ns]$ and a maximum energy of 200 $[mJ]$. The laser beam is directed parallel to the bottom of the water tank, as shown in Figure 2. The beam passed a negative lens to form a 5 $[mm]$ thin laser sheet. The laser is triggered by a camera and operates at $29[Hz]$.

The recording is performed by a CCD camera (Kodak Megaplus, 10-bit ES1.0, 1008×1019 $[pixels]$). The camera records images at a maximum frame rate of $29[Hz]$. A Nikon lens with a focal distance of $50[cm]$ is used in front of the CCD camera. A detailed description of the image recording and post-processing system is given by Ren *et al.* (2003).

Investigation techniques

Visualization method

Flow visualizations are carried out using an electro-chemical tin-precipitation method. In this method tin-ions are separated from an anode, by applying a voltage difference. In the current set-up a thin tin wire which is used as an anode is positioned upstream of the cylinder. Because the tin-ions don't dissolve in pH-neutral water, the small tin-hydroxide particles of $\mathcal{O}(1[\mu m])$ form a homogeneous sheet

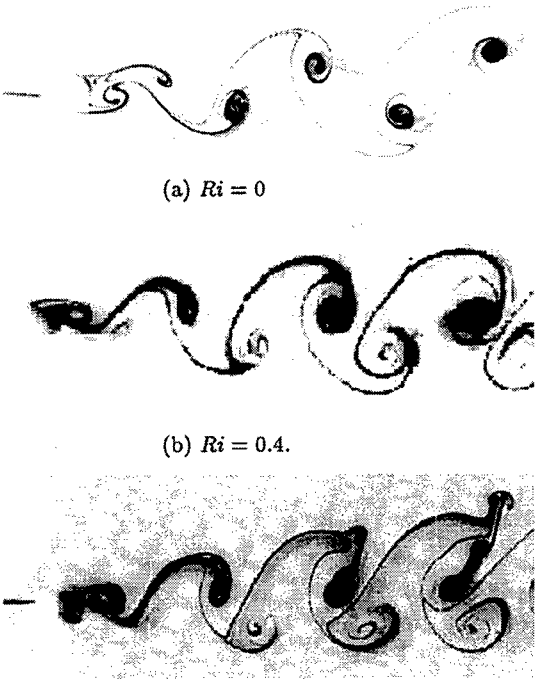

(a) $Ri = 0$

(b) $Ri = 0.4$.

(c) $Ri = 1.0$.

Figure 3: Side-view of the wake flow at $Re = 117$ and various Richardson numbers.

that moves towards the cylinder. With this sheet the wake behind the cylinder is visualized. A detailed description of the visualization method is presented in Maas *et al.* (2003).

3D Spectral Element Method

3D numerical simulations are performed using a Spectral Element Method. A convection-diffusion splitting method is used for the time discretization. The convection equation is solved by a three-steps explicit Taylor-Galerkin scheme. The diffusion equation is discretized by an implicit second-order backward difference scheme. Within an element, the equations are discretized using a 5th-order Spectral Method. The computational domain has dimensions $length \times height \times width = 15d \times 7d \times 4d$.

For the boundary conditions, a normal velocity of zero is prescribed at the side, top and bottom walls. At the outflow wall, a normal-stress-free condition is used. Besides, tangential stresses are set to zero at these walls. At the inlet Dirichlet boundary conditions are applied for velocity components. For the boundaries on which the normal velocity is prescribed by a Dirichlet condition, the boundary conditions for the pressure correction term follow immediately from global mass conservation (Timmermans *et al.* 1996). At the cylinder wall no-slip conditions are applied, while the dimensionless temperature is set to one (Ren *et al.* 2003).

3D-TRANSITION BEHIND A HEATED CYLINDER

Qualitative observations

The influence of a heat input on the 3D wake transition is studied by an electro-chemical tin-precipitation visualization experiment. The experiments are performed at different Richardson numbers.

Side-view of the wake

For $Ri = 0$ and $Re = 117$, the wake flow manifests itself as the von Kármán vortex street, as shown in Figure

3(a). If one increases the input of heat, say to $Ri = 0.4$, the wake still resembles more or less the von Kármán vortex street, as shown in Figure 3(b). Generally, for $Ri < 1$, the heat is initially captured in the core of the shed vortices, and only diffusion processes can cause it to spread. Because water is used as the working fluid, the diffusion take places relatively slow and the vortex street remains primarily two-dimensional (2D).

If one again increases the heat input, for $Ri > 1$ the upward buoyancy force seems to change the flow pattern of the upper vortices. Thermal plumes are being formed and escape in the far-wake, as shown in Figure 3(c).

Top-view of the wake

Next, the camera is positioned above the cylinder with some angle and the corresponding top-view of flow pattern is presented. It clearly shows the development of the escaping thermal plumes for $Ri = 1.0$, as shown in Figure 4(a). It is observed that the thermal plumes are initiated in the near-wake and escape from the upper vortices in the far-wake. The thermal plumes occur at certain spanwise positions, and the distance between the plumes is around twice the cylinder diameter.

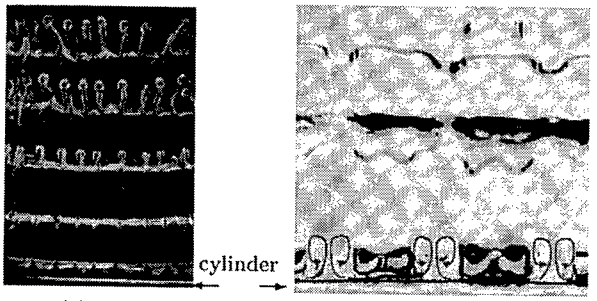

Figure 4: (a) Top-view of the flow pattern behind the cylinder for $Ri = 1.0$ and $Re = 117$; (b) Visualization of the counter-rotating vortices directly behind the cylinder.

To understand the formation of the thermal plumes, detailed visualizations are conducted in the near-wake. By cutting the wake with a horizontal laser sheet, a top-view of the wake flow is recorded. It is observed that pairs of counter-rotating vortices appear directly behind the cylinder, as shown in Figure 4(b). The distance between the counter-rotating vortices is exactly the same as the distance between the plumes, being twice the cylinder diameter.

Furthermore, the spanwise positions of the counter-rotating vortices determine the positions at which the thermal plumes escape in the far-wake. The observations suggest a strong link between the escaping thermal plumes and the counter-rotating vortices occurring in the near-wake. Likewise, experimental observations show that the counter-rotating vortices appear for $Ri > 0.3$ ($Re = 117$). A High resolution Particle Velocimetry (HPV) measurement shows the quantitative details of the counter-rotating vortices with a high resolution, which is presented in Ren *et al.* (2002).

Quantitative observations

A 3D-SEM simulation provides insight into the occurrence of the counter-rotating vortices in the near-wake. A snapshot of pairs of the counter-rotating vortices are presented in Figure 5, where the iso-vorticity surface $\omega_y = \pm 0.8$ (vorticity component in gravity direction) are plotted. These pairs of the counter-rotating vortices are formed directly behind the cylinder. The center of the counter-rotating vortices is located at $Z = -4$, $Z = -2$ and $Z = 0$. The 3D-SEM results agree quite well with the visualization results. The distance between the counter-rotating vortices is two cylinder diameters. In Figure 5, dimension is based on the cylinder diameter and in the remainder of the text all dimensions are scaled with the cylinder diameter.

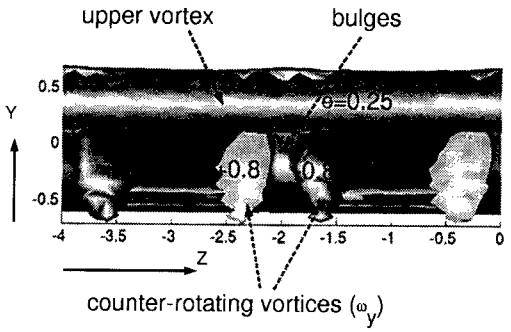

Figure 5: A three-dimensional snapshot of the counter-rotating vortices (iso-vorticity surface of $\omega_y = \pm 0.8$) for $Re = 85$ and $Ri = 1.0$ from a front-view. The iso-temperature surface $\Theta = 0.25$ is shown as a reference. The center region of the counter-rotating vortices has a high temperature and is indicated as "bulges".

To understand the formation of the 3D vortical structures in the near-wake, the streamwise vorticity component ω_x is analyzed. The development of this component is presented in Figure 6 with a top-view. The lower vortices are also plotted as a reference in the shaded background by iso-vorticity surface of ω_z.

As shown in Figure 6, a pair of counter-rotating vortices is located around $Z = -2$. It is observed that the vortices "CRP" & "CRN" have roughly the same but opposite strength. "CRP" & "CRN" (Counter Rotating Positive/Negative vortices) are marked with sign "+/−" representing positive/negative vorticity strength. Furthermore, the strength of the counter-rotating vortices increases with time and the vortices are stretched by the shear layer, as shown in Figure 6 (a)-(d). The distance between the pair of counter-rotating vortices is around twice the cylinder diameter.

Likewise, the counter-rotating vortices "CRP" & "CRN" are stretched by the shear layer and further develop into two parts. One of them is pulled into the upper half of the wake and becomes "UP1" & "UN1" (Upper Positive/Negative part), as indicated in Figure 6 (a). The corresponding side-view of the formation of "UP1" & "UN1" is shown in Figure 7 (a). At $t = T/4$, the shear layer from the other side of the wake cross the centerline of the wake, and cuts off the supply of vorticity from the wall, as described by Green & Gerrard (1993). In Figure 7 (b), the "UP1" & "UN1" will be pulled into the upper strand (stagnation point), where the strain field reaches its maximum. It is observed that the "UP1" & "UN1" almost disappear by the action of the strain field and that new counter-rotating vortices "UP2" & "UN2" are just formed directly behind the cylinder, as shown in Figure 6 (c) & 7 (c). Furthermore, "UP2" & "UN2" will develop in a similar fashion as "UP1" & "UN1".

The second part of the counter-rotating vortices "CRP" & "CRN" is evolved into the lower half of the wake and they are indicated as "LP2" & "LN2" (Lower Positive/Negative part). It is observed that the "LP2" & "LN2" are further stretched and pulled into the lower strand. The streamwise vorticity of those filaments left in the lower braid will be amplified, as shown in Figure 7 (a)-(d). It should be men-

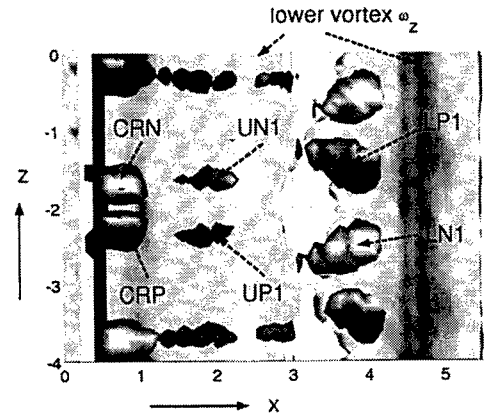

(a) $t = 0$

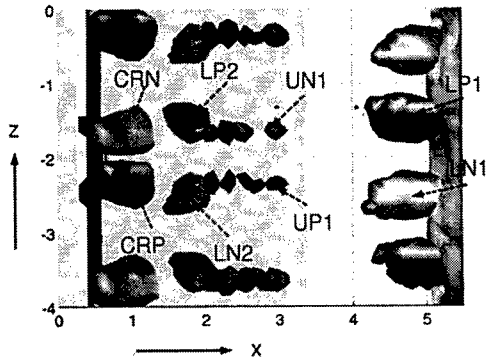

(b) $t = T/4$

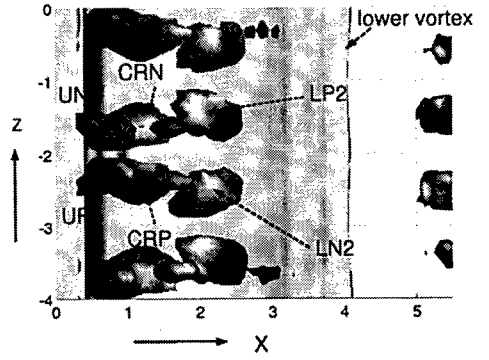

(c) $t = 2T/4$

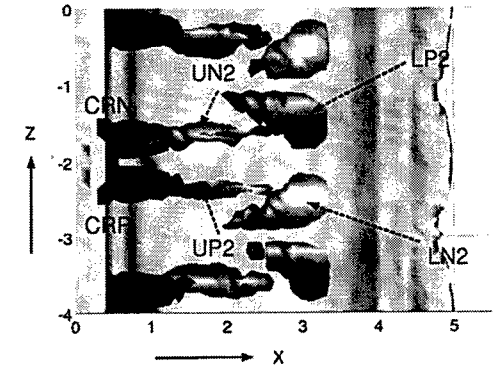

(d) $t = 3T/4$

Figure 6: Top-view: 3D iso-vorticity surface ω_x (component in streamwise direction) for $Re = 85$ and $Ri = 1.0$. The lower vortices are presented as a reference in the shaded background with an iso-vorticity surface of ω_z (component in spanwise direction).

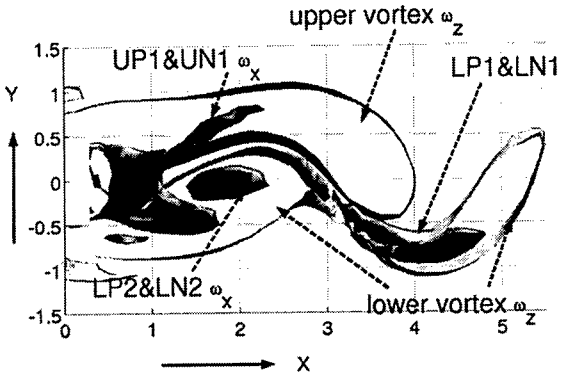

(a) $t = 0$

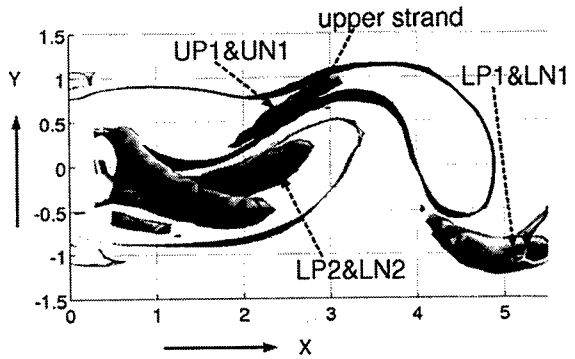

(b) $t = T/4$

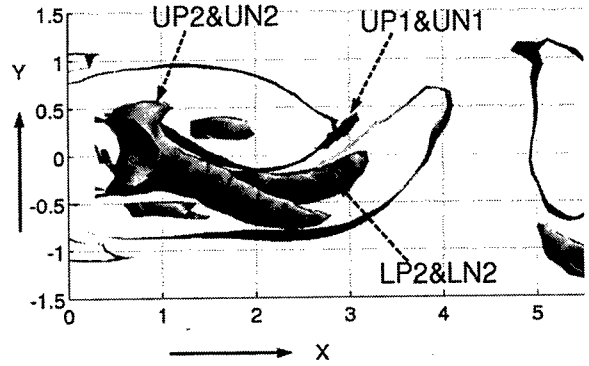

(c) $t = 2T/4$

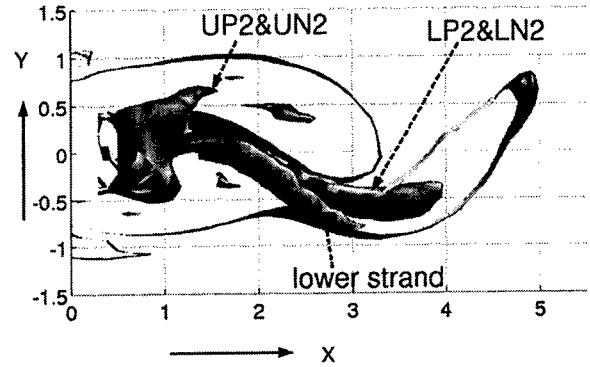

(d) $t = 3T/4$

Figure 7: Side-view: 3D iso-vorticity surface ω_x (component in streamwise direction) and ω_z (component in spanwise direction) for $Re = 85$ and $Ri = 1.0$.

tioned that "LP2" & "LN2" will develop in a similar fashion as "LP1" & "LN1".

Comparing the processes in the upper half and the lower half of the near-wake, the numerical results indicate that the development of the streamwise vorticity of the resulting filaments differs quite a lot. With the action of the strain field, the streamwise vorticity filaments in the upper half of the wake are weakened and the ones in the lower half of the wake are strengthened.

A similar interaction has been observed in Mittal *et al.* (1995) who demonstrated the streamwise vorticity generation in the forced convection case for $Re = 525$ by 3D DNS. The stretching of a small scale perturbation in the near-wake results in streamwise rib-like structures in the braid. The strength of the streamwise vorticity is amplified in the braid by the action of the local strain field.

Temperature field in the near-wake

Due to the interaction between forced convection and buoyancy induced convection, the resulting flow pattern behind the heated cylinder has changed significantly.

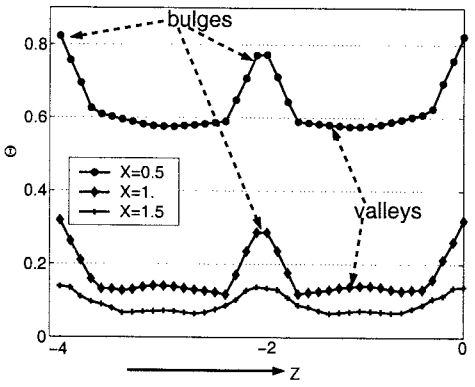

Figure 8: Numerically calculated temperature profiles at the positions $X = 0.5, 1.0, 1.5$ and $Y = 0$ for $Re = 85$ and $Ri = 1.0$.

It is observed that there is a non-uniform temperature distribution along the spanwise direction. In Figure 8 the temperature distribution is presented at different streamwise positions in the center-plane ($X = 0.5, 1.0, 1.5$ and $Y = 0$). The fluid at the position "bulges" has a higher temperature than the fluid at the position "valleys". In the near-wake, at intersection $X = 0.5$, the spanwise temperature difference between "bulges" and "valleys" is around 0.3. The spanwise temperature difference becomes less and the temperature decreases in streamwise direction, as can be concluded from the temperature profiles at the intersections $X = 0.5, 1.0, 1.5$.

In Figure 9 3D iso-temperature surface is shown. The spanwise temperature distribution is observed as "bulges" and "valleys" which are formed directly behind the cylinder, see Figure 9 (a). These "bulges" develop with time. Part of the heat is convected downstream together with the upper and lower vortices and part of the heat is used to form rib-like structures, as shown in Figure 9 (b).

Furthermore, the spanwise temperature distribution of the lower vortices is strongly deformed, as shown in Figure 9 (c). However, the temperature in the core of the upper vortices remains primarily two dimensional (2D).

Despite the relative low heat diffusion ($Pr = 7$), the heat captured in the lower vortices ends up in three warm blobs, as demonstrated in Figure 9 (d). Meanwhile, new "bulges" and "valleys" are just formed directly behind the cylinder.

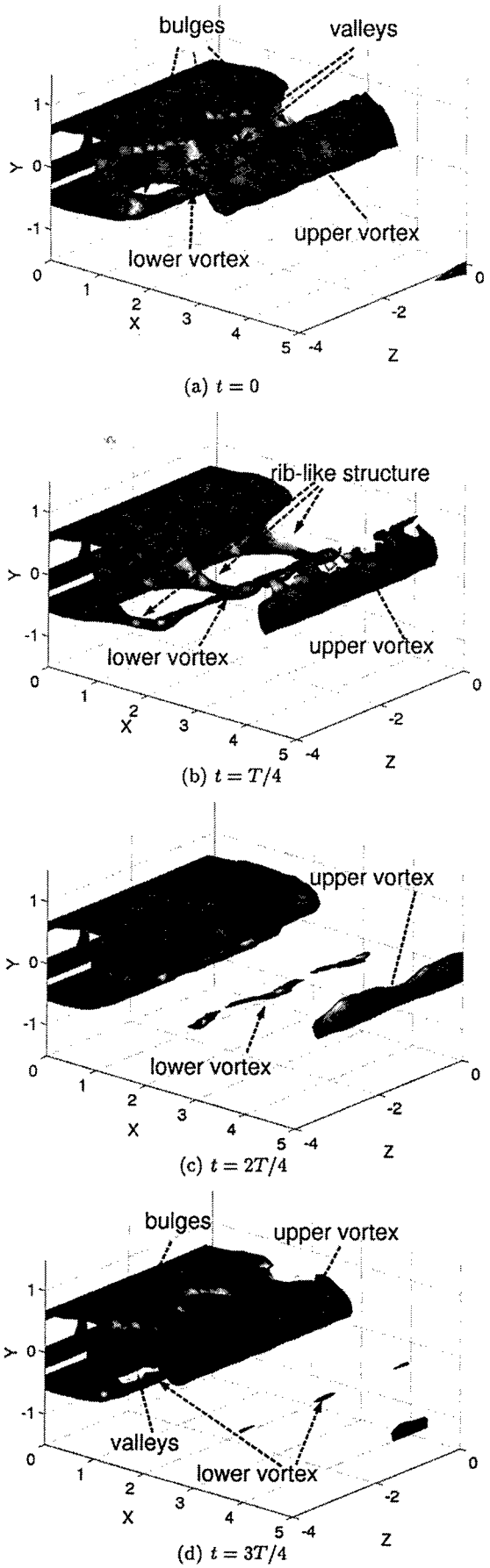

Figure 9: Numerically calculated 3D iso-temperature surface $\Theta = 0.25$ for $Ri = 1.0$ and $Re = 85$.

Baroclinic vorticity production

A non-uniform spanwise temperature distribution is observed along the spanwise direction, as shown in Figure 8. The temperature field is presented as "bulges" and "valleys" directly behind the cylinder. The 3D vortical structures can be explained by the baroclinic production term in the variable-density vorticity transport equation.

$$\frac{D\omega}{Dt} = \omega \cdot \nabla \mathrm{u} + \frac{1}{\rho^2}(\nabla\rho \times \nabla p) + \nu\nabla^2\omega \qquad (4)$$

The baroclinic torque is the cross production term. Although there is a density variation in this equation, the flow is considered incompressible. Inviscidly, the pressure gradient can be expressed:

$$\nabla p = -\rho\frac{Du}{Dt} + \rho\mathbf{g} \simeq \rho\mathbf{g} \qquad (5)$$

The inertial component of the pressure gradient turns out to be much less than the hydrostatic portion. Thus ∇p is always directed downwards. The temperature gradient has an opposite sign in comparison to the density gradient $\nabla T \sim -\nabla\rho$.

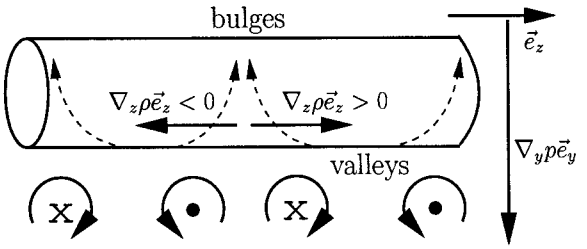

Figure 10: Sketch of the streamwise vorticity ω_x generated by the action of baroclinic production. The points and crosses represent the rotation direction.

Considering the flow behind the cylinder, the density gradient has a positive/negative sign along the spanwise direction. Streamwise vorticity ω_x is generated by the action of the baroclinic torque

$$\nabla_z\rho\vec{e}_z \times \nabla_y p\vec{e}_y = \frac{\partial\rho}{\partial z}\vec{e}_z \times \frac{\partial p}{\partial y}\vec{e}_y \qquad (6)$$

where ∇_z stands for the gradient in the Z direction and $\vec{e}_z$ is the unit vector in the Z direction. As indicated in Figure 10, the density increases along the spanwise direction from "bulges" to "valleys" ($\nabla_z\rho\vec{e}_z > 0$). As shown in Figure 10, the points and crosses represent the rotation direction: outward and inward of the paper. It corresponds to the directions found in Figure 6.

Furthermore, the temperature decreases also in streamwise direction, as observed in Figure 8. The density gradient in the near-wake is positive in streamwise direction ($\nabla_x\rho\vec{e}_x > 0$), and an additional clockwise spanwise vorticity ω_z' is created due to the cross production $\nabla_x\rho\vec{e}_x \times \nabla_y p\vec{e}_y$. If the baroclinic torque has the same sign as the local vortices the vortices are strengthened. Similarly, if the baroclinic torque has the opposite sign as the local vortices the vortices are weakened. It is observed that the strength of the upper vortices is much stronger than the lower ones, which is agreement with the 2D numerical simulations observations by Kieft *et al.* (2003).

CONCLUSIONS

For a Reynolds number around 100, it is observed that, for $Ri > 1.0$, thermal plumes escape from the upper braid in the far-wake. These thermal plumes are associated with pairs of counter-rotating vortices in the near-wake. The pairs of counter-rotating vortices appear for $Ri > 0.3$ ($Re = 117$). The strength of these counter-rotating vortices is depending on the value of the Richardson number.

From a numerical analysis it is observed that the counter-rotating vortices are stretched and pulled into two parts, and that they are stretched into the braids. It is quite remarkable that during this process the streamwise vortices filaments are weakened in the upper braid and strengthened in the lower ones.

In the near-wake, a non-uniform temperature distribution in spanwise direction is found. The temperature field is presented as "bulges" and "valleys" directly behind the cylinder. This suggests that the 3D vortical structures are associated with the non-uniform temperature distribution along the spanwise direction in the near-wake. Streamwise counter-rotating vortices ω_x are generated by the baroclinic torque $\nabla_z\rho\vec{e}_z \times \nabla_y p\vec{e}_y$. Besides that, due to the generation of an additional clockwise spanwise vorticity ω_z' by the baroclinic torque $\nabla_x\rho\vec{e}_x \times \nabla_y p\vec{e}_y$, the strength of the upper vortices becomes stronger than the lower ones. This leads to an early break down of the von Kármán vortex street.

ACKNOWLEDGMENTS

This work is part of the research programme of the Netherlands Foundation for Fundamental Research on Matters (FOM), which is financially supported by the Netherlands Organization for Scientific Research (NWO). The authors would like to thank the secretaries and technical staffs of the Section Energy Technology of the Department of Mechanical Engineering, in Eindhoven University of Technology for their support.

REFERENCE

Green, R.B. & Gerrard, J.H. (1993). Vorticity measurements in the near wake of a circular cylinder at low Reynolds numbers, *J. Fluid Mech.*, **246**, 675

Kieft, R.N., Rindt, C.C.M. & van Steenhoven, A.A. (2002). Heat induced transition of a stable vortex street. *Int. J. Heat Mass Transfer*, **45**, 2739

Kieft, R.N., Rindt, C.C.M., van Steenhoven, A.A. & van Heijst, G.J.F. (2003), On the wake structure behind a heated horizontal cylinder in cross-flow, *J. Fluid Mech.*, (accepted)

Maas. W.J.P.M., Rindt, C.C.M. & van Steenhoven, A.A. (2003). The influence of heat on the 3D-transition of the Von Kármán-Vortex street. *Int. J. Heat Mass Transfer*, (accepted)

Mittal, R. & Balachander, S. (1995). Generation of streamwise vortical structures in bluff-body wake. *Phys. Rev. Lett.*, **75**, 1300

Ren, M., Rindt, C.C.M. & van Steenhoven, A.A. (2002). The influence of heat on the 3D-transition of the cylinder wake flow, *Proc. 12th International Heat Transfer Conference*, Grenoble, France

Ren, M., Rindt, C.C.M. & van Steenhoven, A.A. (2003). 3D vortices in the wake flow behind a heated cylinder, *Proc. EUROTHERM 74 in Heat transfer in unsteady and transitional flows*, Eindhoven, The Netherlands

Timmermans, L.J.P, Minev, P.D. & van de Vosse, F.N. (1996) An approximate projection scheme for incompressible flow using spectral elements. *Int. J. Numer. Meth. Fluids*, **22**, 673

Williamson, C.H.K. (1996). Three-dimensional wake transition. *J. Fluid Mech.*, **328**, 345